J. Fluid Mech. (2017), *vol.* 828, *pp.* 57–69.
doi:10.1017/jfm.2017.520

Aspect ratio effect on electroconvection in a suspended liquid crystal film with a rectangular boundary

Xuefei Guo[1], Yongkang Le[1] and Bochao Cao[2,†]

[1]Department of Physics, Fudan University, Shanghai 200433, China

[2]Department of Aeronautics and Astronautics, Fudan University, Shanghai 200433, China

(Received 6 April 2017; revised 2 June 2017; accepted 24 July 2017;
first published online 31 August 2017)

The aspect ratio dependence of the electroconvection phenomenon in a suspended nematic liquid crystal film with a rectangular boundary is investigated. Two-dimensional global stability analysis is carried out on the coupled electrohydrodynamic system to calculate the instability boundary of the phenomenon for different aspect ratios. The calculated critical R number (Rayleigh-like number) shows a rapidly decreasing trend in the low-aspect-ratio region (roughly $\gamma < 1.5$, where γ is defined as the aspect ratio of the film), and then the variation becomes slow until $\gamma \approx 2.5$, where the critical R number starts to increase slightly. Convective patterns of liquid films with different aspect ratios are also obtained from stability analysis and validated by particle image velocimetry measurement.

Key words: instability, liquid crystals, thin films

1. Introduction

The electroconvection phenomenon, which exhibits complex temporal and spatial patterns, has been widely investigated by many researchers in the past few decades. Most of the research works have been focused on a sandwich set-up with two parallel flat plates and a thin layer of nematic liquid crystal in the middle. In the presence of an applied electric field perpendicular to the flat plates, spatial free charges can be induced in the liquid crystal due to the anisotropic nature of liquid crystal molecules. Then, the nonlinearity of the coupled electrohydrodynamic system can result in many convective patterns (such as normal rolls, oblique rolls or travelling rolls, etc.) in the liquid crystal layer of this sandwich configuration (Cross & Hohenberg 1993; Kramer & Pesch 1995; Buka *et al.* 2007).

However, due to the existence of two plates, the resulting convective flow in the liquid crystal of the sandwich set-up is highly three-dimensional, which makes the analysis very complicated. To remove the influence of the two plates, Faetti, Fronzoni & Rolla (1983) came up with another set-up with liquid crystal suspended on a rectangular boundary, and the electroconvection phenomenon was then investigated in

† Email address for correspondence: cbc@fudan.edu.cn

this suspended liquid crystal thin film where the flow motion could be approximately viewed as two-dimensional. They observed the formation of vortex patterns with certain spatial periodicity in the liquid crystal film when AC or DC voltage was applied. In this suspended film set-up, the free charges are mainly induced by a surface charge mechanism instead of anisotropy of the liquid crystal molecules. Subsequently, a series of research works have been carried out with respect to the electroconvection problem in a suspended liquid crystal film system. A highly two-dimensional system was realized by Morris, Bruyn & May (1990) by using smectic liquid crystal instead of nematic liquid crystal in their suspended thin film, since smectic layering can further constrain the flow of the third dimension and help to reduce the thickness variation of the film. In the experiment, they found that both DC and AC coupled set-ups can result in similar instability phenomena. Tsai, Daya & Morris (2004) changed the experimental set-up from a long (very-large-aspect-ratio) rectangular film (Faetti *et al.* 1983; Morris *et al.* 1990) to an annular shaped thin film. Therefore, the one-dimensional periodicity of the problem is perfectly retained and at the same time the aspect ratio of the set-up can be adjusted by changing the radius of the inner or outer circle. Using this set-up, they investigated the aspect ratio dependence of turbulent electroconvection. Daya, Deyirmenjian & Morris (1999) applied additional Couette shear to the annular thin film set-up by rotating the inner edge of the film, so another control parameter, the rotational Reynolds number, was added into the system. They found that this additional control parameter can help to adjust the neutral stability boundary of the system. Further investigations were carried out on this annular system with or without Couette shear by direct numerical simulation (Tsai *et al.* 2007; Tsai, Morris & Daya 2008). More flow visualization results of this electroconvection phenomenon have been revealed in these numerical studies.

Thus far, a great deal of effort has been put into research on electroconvection in suspended liquid crystal films. However, to simplify the problem, one-dimensional periodicity has been introduced in most of the previous experiments either by making the rectangular film very slender (large aspect ratio) or by using an annular shaped set-up and correspondingly assuming a certain wavenumber along one direction in the analysis. In the current work, a complete two-dimensional global stability analysis is carried out on the rectangular liquid crystal film. Instability of the electrohydrodynamic system with different aspect ratios is discussed. The development of a two-dimensional flow pattern on the liquid film as the aspect ratio varies is investigated through stability analysis. Moreover, to validate the results obtained from stability analysis, the convective flow on the film is quantitatively measured through a particle image velocimetry (PIV) experiment.

2. Experimental set-up

In the experiment, a liquid crystal film is suspended on a rectangular frame which is set up using two conductive molybdenum wires and two insulated nylon wires, as shown in figure 1. The diameters of the molybdenum wires and nylon wires are both 0.1 mm. The dimensions d and L vary in the ranges 2–6 mm and 3–14 mm respectively. The liquid crystal is 4'-n-octylbiphenyl-4-carbonitrile (8CB) (99 %, J&K Scientific) and the experimental temperature of the liquid film area is kept at 34 °C, so that the liquid crystal can stay in the nematic phase (Sharma, MacDonald & Iannacchione 2006). The average thickness of the film is $\bar{s} = 25$ μm, the conductivity of the liquid crystal is $\sigma = 5 \times 10^{-8} (\Omega^{-1}\ \mathrm{m}^{-1})$, the viscosity is $\eta = 0.1$ kg (s m)$^{-1}$

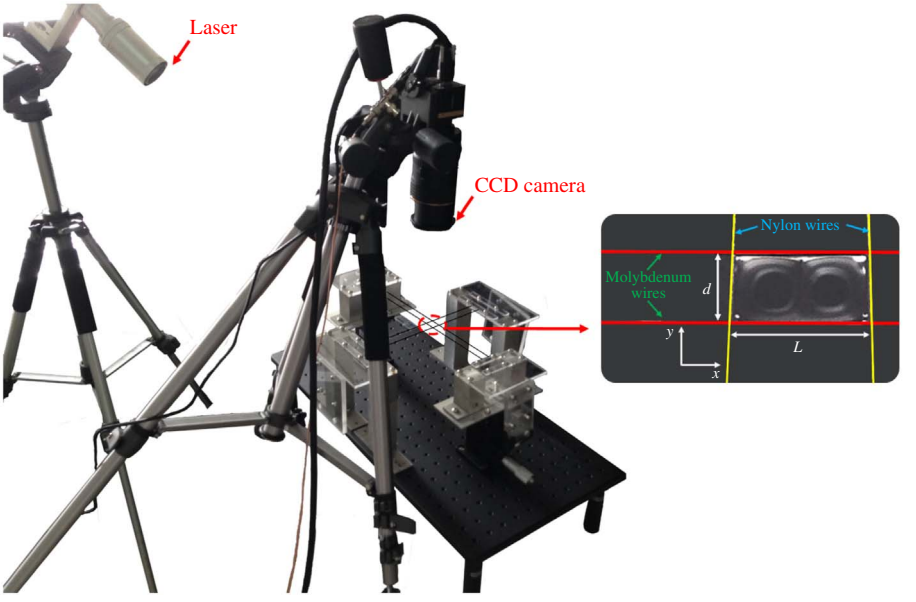

FIGURE 1. (Colour online) Experimental set-up.

and the mass density is $\rho = 1.0 \times 10^3$ kg m^{-3} (Morris, Bruyn & May 1991; Patrício *et al.* 2012). Here, the average thickness of the film is estimated by the value of the volume of the liquid crystal used to make the film divided by the area of the film. A DC voltage is applied between the molybdenum wires to drive the liquid film to move. To measure the flow field in the liquid film, a PIV experiment is carried out. In the experiment, fluorescent particles with diameters of 1–2 μm are added to the liquid crystal film to track the motion of the fluid. To ensure the uniformity of the tracking particles in the film, the fluorescent particles are premixed with the liquid crystal using an ultrasonic mixer at a temperature of 50 °C before the experiment. A pulsed Nd : YAG laser with an energy of 200 mJ and a frequency of 5 Hz is used to excite the fluorescence of the particles, and flow field images are captured by a CCD camera with a resolution of 2456 × 2058. In this work, all of the results obtained from PIV measurements are averaged results of 100 flow field images.

In previous experimental work, researchers used liquid crystal in the smectic phase instead of the nematic phase to make thin (10^{-2}–10^{-1} μm) and stable film (Morris *et al.* 1990; Becker *et al.* 1997), which is a very good two-dimensional system. However, in the current PIV experiment, fluorescent tracking particles with diameters of 1–2 μm have to be evenly distributed in the liquid crystal film. Thus, we have to make a film with a thickness of tens of microns using nematic liquid crystal to realize the PIV measurements, although the thickness variation of a nematic liquid crystal film could affect the two-dimensionality of the system, as can be noted in figure 1. As reported by Faetti *et al.* (1983), two different types of flow patterns can be observed in a suspended nematic liquid crystal film, which are named as the domain mode and the vortex mode respectively. The domain mode results from a Carr–Helfrich mechanism in the anisotropic phase of the nematic liquid crystal, while the vortex mode is mainly driven by a surface charge mechanism. In this work, only the vortex mode (vortical flow pattern) is investigated and discussed.

3. Linear stability analysis

The current analysis is based on a physical model similar to the ones proposed in previous works (Melcher & Taylor 1969; Daya, Morris & Bruyn 1997; Feiz, Namin & Amjadi 2015). It is assumed that the fluid motion in the liquid crystal film is restrained in two dimensions, which means that the convection in the third dimension inside the film is neglected. Due to the electric potential difference between the liquid crystal film surface and the surrounding air, free charges are induced at the surface of the film near the electrodes with the same signs, and they move in the film under the effects of fluid convection and the electric field induced by the electrodes. On the other hand, electric force resulting from distributed charges drives motion of fluids. Finally, a certain flow pattern could result in the liquid film after this coupling effect between the electric and flow fields has converged to a stable state. According to the above physical assumptions, this 2D coupling system can be described by the charge continuity equation and the incompressible Navier–Stokes equation, and they can be written in dimensionless form as follows:

$$\frac{\partial q_s}{\partial t} + \boldsymbol{\nabla} \cdot (\boldsymbol{E}_s + q_s \boldsymbol{u}) = 0, \tag{3.1}$$

$$P^{-1}\left(\frac{\partial(\nabla^2\psi)}{\partial t} + \frac{\partial\psi}{\partial y}\frac{\partial(\nabla^2\psi)}{\partial x} - \frac{\partial\psi}{\partial x}\frac{\partial(\nabla^2\psi)}{\partial y}\right) - \nabla^4\psi = -R\left[\frac{\partial(q_s E_{sy})}{\partial x} - \frac{\partial(q_s E_{sx})}{\partial y}\right], \tag{3.2}$$

where q_s denotes the surface charge density, $\boldsymbol{E}_s$ is the electric field intensity projection on the liquid film, $\boldsymbol{u}$ is the fluid velocity and ψ is the stream function. Since the controlling equations are written in two-dimensional form, all of the material parameters are given in areal form as $\eta_s = \eta s$, $\rho_s = \rho s$ and $\sigma_s = \sigma s$, where s is the thickness of the film. In (3.1) and (3.2), lengths and times are non-dimensionalized by d and $\varepsilon_0 d/\sigma s$ respectively, and the characteristic charge density is set as $\varepsilon_0 U/d$, where ε_0 is the vacuum permittivity, d is the distance between the two electrodes and U is the potential drop between the two electrodes. The two dimensionless parameters, P and R, are analogous to the Prandtl number and Rayleigh number in the Rayleigh–Bénard convection problem, and are as defined below:

$$P = \frac{\varepsilon_0 \eta}{\rho \sigma s d}, \tag{3.3}$$

$$R = \frac{\varepsilon_0^2 U^2}{\eta \sigma s^2}. \tag{3.4}$$

Moreover, the surface charge q_s and electric potential ϕ are coupled through the 3D Laplace equation, $\nabla^2\phi = 0$, with boundary condition $q_s = -2(\partial\phi/\partial z)|_{z=0^+}$ (z is the normal direction of the liquid film surface) according to the Maxwell equation expressed in the 3D domain above the liquid crystal film. In this work, stability analysis is carried out with respect to the equilibrium state of the static liquid film with static charge distribution when DC voltage is applied on the electrodes. Thus, the base state of the fluid flow is $\boldsymbol{u} = 0$ everywhere. To calculate the base state of the charge density distribution q_s, a linear electric potential drop is assumed between the two electrodes and the 3D Laplace equation is numerically solved using the second-order central difference method. To validate the computational results, the charge density distribution along a line in the middle of the film is taken to compare

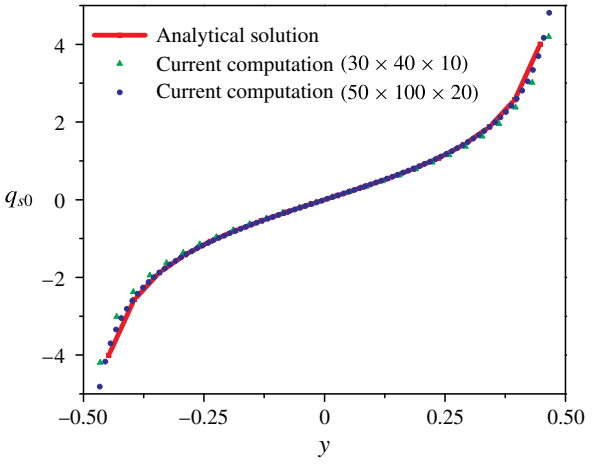

FIGURE 2. (Colour online) Comparison of the analytical solution (Daya *et al.* 1997) and the current computations for surface charge distribution.

with the 2D analytical solution, as given by Daya *et al.* (1997). Moreover, to test the grid convergence, two different sets of grids ($30 \times 40 \times 10$ and $50 \times 100 \times 20$, which in the 2D liquid film are 20×30 and 40×90 respectively) are used in the computation. In the validation test, the film aspect ratio is set as $\gamma = 2$ ($\gamma = L/d$, where L is the distance between the two insulated wires, as shown in figure 1). As shown in figure 2, the computed charge density distribution matches with the analytical solution very well and it does not vary with grid density. Therefore, in the remainder of the paper, a grid of $30 \times 40 \times 10$ is used in all of the computations.

In the stability analysis, small perturbations with temporal growth are assumed and superimposed onto base physical quantities as follows:

$$\phi = \phi_0(x, y) + \phi_1(x, y)\mathrm{e}^{\lambda t}, \tag{3.5}$$

$$q_s = q_{s0}(x, y) + q_{s1}(x, y)\mathrm{e}^{\lambda t}, \tag{3.6}$$

$$\psi = \psi_0(x, y) + \psi_1(x, y)\mathrm{e}^{\lambda t}, \tag{3.7}$$

where ϕ_0, q_{s0}, ψ_0 are base state physical quantities and ϕ_1, q_{s1}, ψ_1 are spatial distributions of small perturbations; λ is the temporal growth rate of perturbations. Since the base state for the current analysis is the static equilibrium of the liquid crystal film, we have $\psi_0 = 0$ everywhere, and ϕ_0 and q_{s0} can be solved from the 3D Laplace equation, as described previously. By substituting these perturbed quantities into the controlling equations (3.1) and (3.2) and neglecting higher-order term, linearized equations are obtained as follows:

$$\nabla^2\phi_1 + \left(\frac{\partial q_{s0}}{\partial y}\frac{\partial \psi_1}{\partial x} - \frac{\partial q_{s0}}{\partial x}\frac{\partial \psi_1}{\partial y}\right) = \lambda q_{s1}, \tag{3.8}$$

$$\nabla^4\psi_1 + R\left(\frac{\partial q_{s0}}{\partial x}\frac{\partial \phi_1}{\partial y} - \frac{\partial q_{s0}}{\partial y}\frac{\partial \phi_1}{\partial x} + \frac{\partial q_{s1}}{\partial x}\frac{\partial \phi_0}{\partial y} - \frac{\partial q_{s1}}{\partial y}\frac{\partial \phi_0}{\partial x}\right) = \lambda P^{-1}\nabla^2\psi_1. \tag{3.9}$$

Since the surface charge q_{s1} and electric potential ϕ_1 are also coupled by the linear Laplace equation, as mentioned previously, we use the following procedure

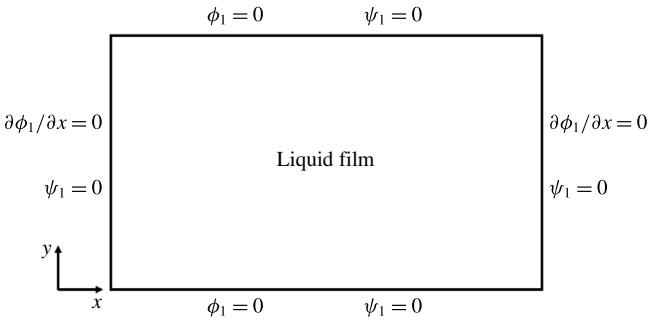

FIGURE 3. Boundary conditions for stability analysis.

(Feiz *et al.* 2015) to relate these two quantities. First, we give an electric potential distribution ϕ_{1ij}, so that $\phi_{1ij} = 1$ at the (i, j) grid point in the liquid film and $\phi_{1ij} = 0$ at the rest of the grid points. Then, a corresponding surface charge distribution $q_{sij}(x, y)$ can be solved from the 3D Laplace equation with a boundary condition of $q_s = -2(\partial\phi/\partial z)|_{z=0^+}$. This routine is repeated for all (i, j) grid points of the liquid film. Finally, for any given electric potential distribution ϕ_1, the corresponding surface charge distribution can be superimposed as $q_{s1}(x, y) = \sum_{i,j} \phi_1(x_{ij}, y_{ij}) q_{sij}(x, y)$. By substituting this relationship into (3.8) and (3.9) and using a second-order central difference scheme to discretize spatial derivatives, finally an eigenvalue problem can be formed. The boundary conditions of this eigenvalue problem are given (Traoré & Pérez 2012) as shown in figure 3.

Eigenvalues with positive real parts ($\lambda_R > 0$) indicate instability of the system, and the corresponding eigenvectors represent unstable spatial modes for the electric and fluid fields.

4. Results and discussion

In the electroconvection problem of a suspended liquid crystal film, as the applied voltage (or the dimensionless parameter R) exceeds a critical value, the static equilibrium of the system is broken and the liquid film starts to move following a certain vortical pattern. This phenomenon has been widely reported in previous work with different film geometries (Faetti *et al.* 1983; Morris *et al.* 1990; Tsai *et al.* 2004). In the current experiment, using the PIV technique, the flow patterns on rectangular liquid films of different aspect ratios are obtained, and the resulting vortical motion is observed to vary with the film aspect ratio γ, as shown in figure 4. Moreover, flow velocity data obtained from the current PIV experiment are substituted into (3.1) to calculate the corresponding electric potential distributions. The calculated electric potential distributions are also plotted in figure 4, and the applied linear electric potential drop between the two electrodes is subtracted from the results.

As shown in figure 4, the number of vortices distributed along the x direction increases from 1 to 4 as the aspect ratio of the liquid film increases from 0.76 to 3.28. Similar vortex patterns are also obtained from stability analysis. Stability analysis is carried out at the same aspect ratios as those set in the experiment, and the unstable eigenmodes for the flow and electric fields are extracted and plotted in figure 5. As shown in figure 5, the obtained unstable eigenmodes match with the experimental results qualitatively well, and they both reveal a trend of an increasing number of vortices as the aspect ratio of the film increases.

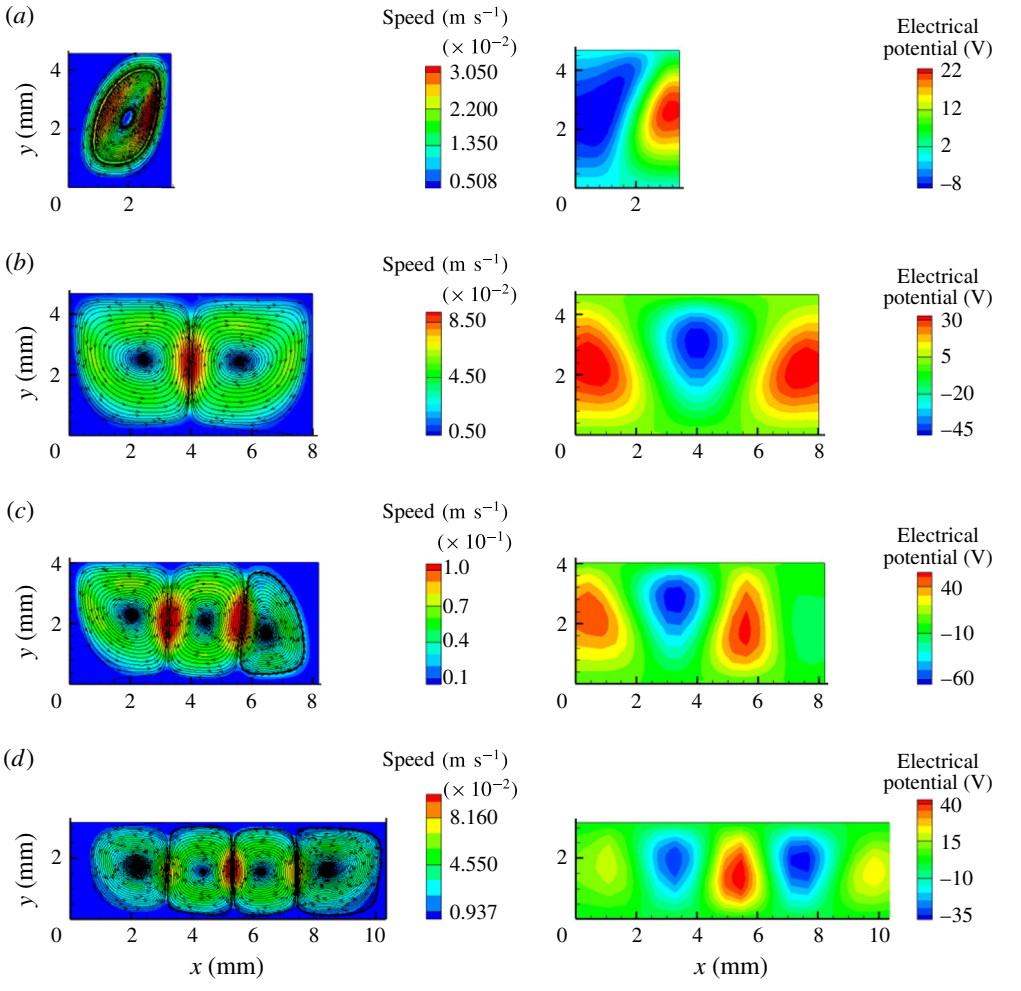

FIGURE 4. (Colour online) Convective patterns obtained from the PIV experiment under different aspect ratios. The left-hand side shows the flow patterns, while the right-hand side shows the patterns of the electric potential (calculated from the measured flow field): (*a*) $U = 1012$ V, $\gamma = 0.73$; (*b*) $U = 818$ V, $\gamma = 1.72$; (*c*) $U = 1014$ V, $\gamma = 2.03$; (*d*) $U = 808$ V, $\gamma = 3.28$.

Through stability analysis, the critical R number (R_c) is calculated for films with different aspect ratios, and the variation of R_c with respect to the film aspect ratio (γ) is investigated. As shown in figure 6, the critical R number decreases almost exponentially with the film aspect ratio for roughly $\gamma < 1.5$, and then the variation becomes slow until $\gamma \approx 2.5$, where R_c starts to increase slightly. Moreover, the flow patterns of the unstable eigenmodes are extracted at different aspect ratios, and boundaries that separate different flow patterns are marked as dashed lines in the plot. As shown in figure 6, the flow pattern boundaries all appear at local maxima of the R_c–γ curve, especially for the low-aspect-ratio region. Similar characteristics of variation of R_c and the flow pattern with respect to the aspect ratio of the rectangular boundary have been reported in computational work by Pérez *et al.* (2014), although the geometry of their problem was sandwich shaped and unipolar injection was the

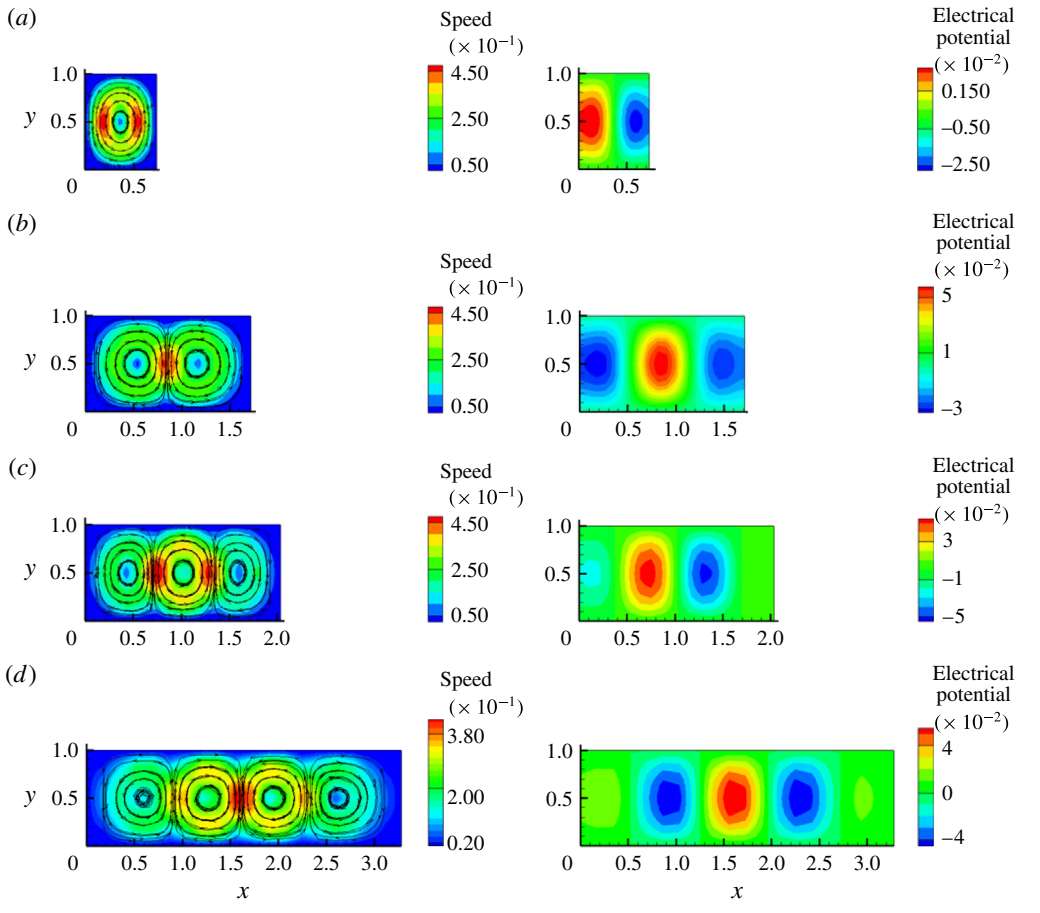

FIGURE 5. (Colour online) Unstable eigenmodes obtained from numerical stability analysis under different aspect ratios. The left-hand side shows the flow patterns, while the right-hand side shows the patterns of the electric potential: (*a*) $R = R_c = 171.1,\ \gamma = 0.73$; (*b*) $R = R_c = 119.3,\ \gamma = 1.72$; (*c*) $R = R_c = 119.5,\ \gamma = 2.03$; (*d*) $R = R_c = 119.3,\ \gamma = 3.28$.

driving mechanism in their physical model. Moreover, with an annular geometry, Daya *et al.* (1999) also found that R_c varies faster at low radius ratios, and local maxima of the R_c curve indicate transition between adjacent flow patterns.

A closer observation of the stability analysis results reveals the whole process of flow pattern variation. As shown in figure 7, when the aspect ratio of the film increases from 1.25 (close to the first flow pattern boundary), vortices start to be stretched gradually in the x direction. Until $\gamma = 1.89$, when vortices are maximumly stretched and the growth of vortices in the x direction stops, a new flow structure starts to appear at one side of the film. As the aspect ratio further increases, this newly emerging flow structure gradually grows into the third vortex with similar dimensions to the other two. Due to the growth of the third vortex, the other two vortices are squeezed in the x direction and their lateral dimension decreases until the third vortex grows to a similar size to them.

In our experiment, it is also observed that the convective pattern shown on the film is not stable at some aspect ratios. At these aspect ratios, the number of vortices

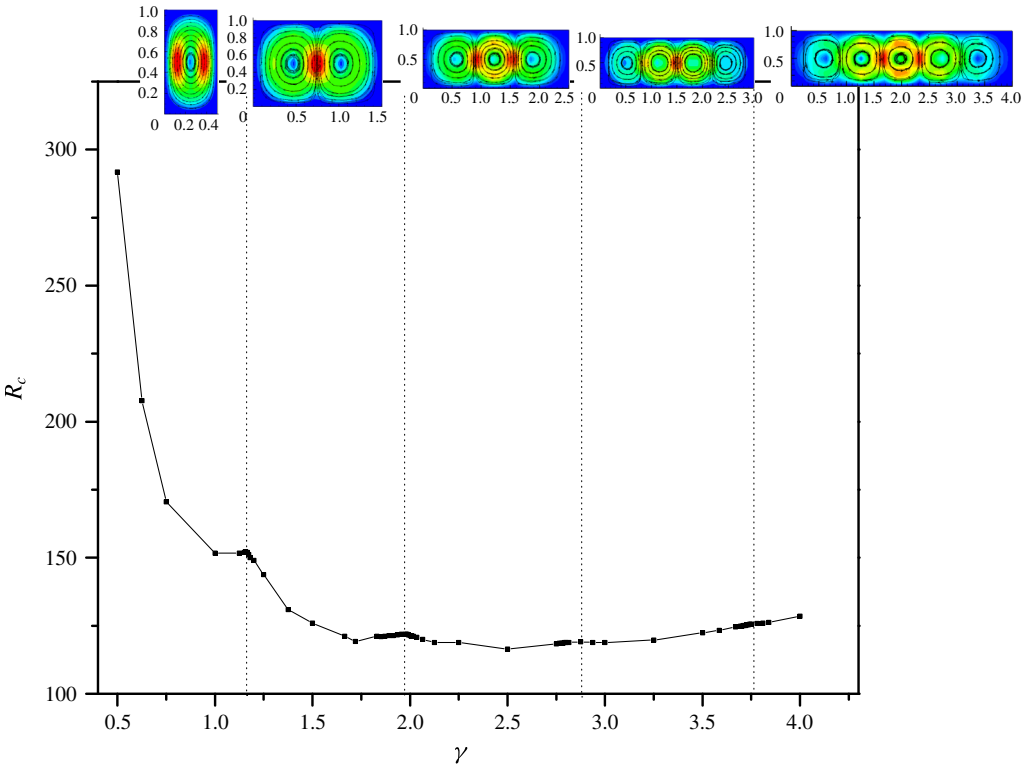

FIGURE 6. (Colour online) Variation of the critical R number with respect to the film aspect ratio.

in the flow pattern switches from m to $m+1$ intermittently. A similar phenomenon has been reported in the earlier work by Faetti *et al.* (1983) and Mao *et al.* (1996) for rectangular films with large aspect ratios ($\gamma > 3$). They observed that the flow pattern is very stable when the lateral dimension (x direction) of the film is close to a multiple of the spatial period of the vortex pattern; otherwise, the flow pattern becomes less stable and vortex structures are created or destroyed at the ends of the film. In the current work, we reinvestigate this problem by stability analysis. In the stability analysis, as the R number further increases beyond the critical value, a new unstable eigenmode can appear at a certain point (second critical R number, R_{c2}). This new unstable flow mode has one more vortex than the previous mode and is always the dominant mode (with larger λ_R), as shown in figure 8. Usually, this new unstable flow mode is not expected to be observed in the experiment because when the applied DC voltage is increased gradually in the experiment, the liquid film has already started to move when the voltage crosses the first critical value, and the base flow for the second stability analysis is no longer static. In this sense, the new unstable flow mode obtained here is spurious and we can only observe one type of flow pattern in the experiment. However, if this second critical voltage (U_{c2}) is very close to the first critical value (U_c), the new unstable mode can behave like a parallel mode of the previous mode and the flow pattern with one more vortex can appear in the experiment if the applied voltage is slightly perturbed. When this happens, the flow pattern shown on the film becomes less stable, as observed in the current experiment and earlier work

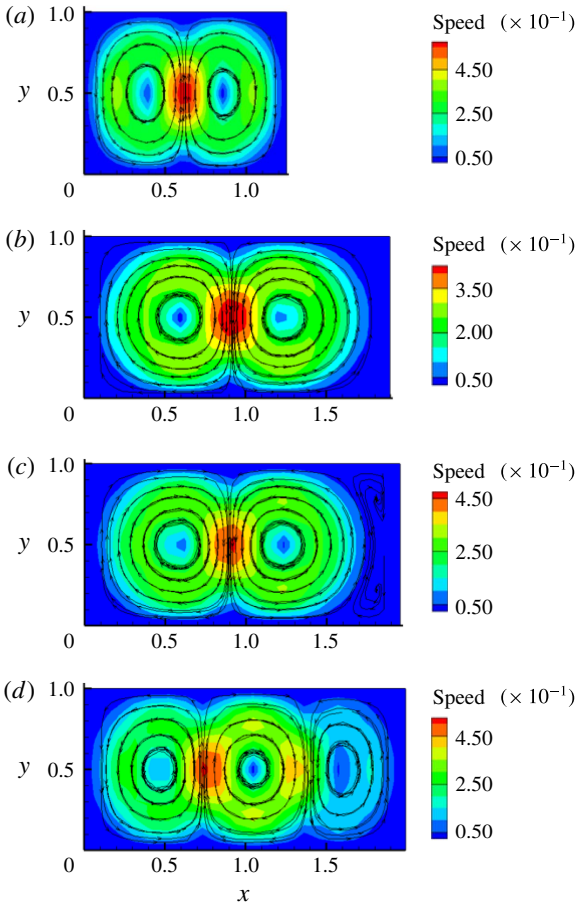

FIGURE 7. (Colour online) The flow pattern variation process as the film aspect ratio increases: (*a*) $R = R_c = 143.75$, $\gamma = 1.25$; (*b*) $R = R_c = 121.43$, $\gamma = 1.89$; (*c*) $R = R_c = 121.91$, $\gamma = 1.96$; (*d*) $R = R_c = 121.67$, $\gamma = 1.99$.

(Faetti *et al.* 1983; Mao *et al.* 1996). In other words, two adjacent linearly unstable modes can indicate instability of the resulting nonlinear flow pattern. In the current analysis, the ratio of the second critical R number to the first critical value (R_{c2}/R_c) is calculated from stability analysis for different aspect ratios, as plotted in figure 9. As can be observed from figure 9, the minima of the R_{c2}/R_c curve are very close to 1 ($1 < R_{c2}/R_c < 1.005$), and they all coincide with the flow pattern boundaries as marked in figure 6. This indicates that the flow pattern shown on the film tends to be less stable when the aspect ratio of the rectangular film is close to the flow pattern boundaries. This is expectable since at these boundaries, the flow pattern is in transition and hence unstable. Similar mode transition behaviour has also been observed in other eletroconvection or hydrodynamic systems with finite aspect ratios. In an experimental work on sheared annular electroconvection, Daya, Deyirmenjian & Morris (2002) observed a convective pattern transition as the R number was tuned up or down from the critical value R_c. Binks & Mullin (1997) reported a mode selection

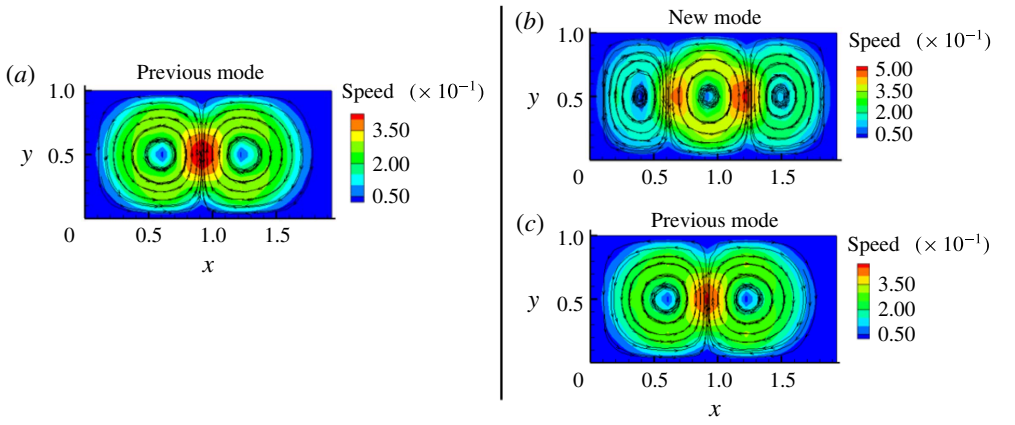

FIGURE 8. (Colour online) Unstable eigenmodes at the first and second critical R numbers with an aspect ratio of $\gamma = 1.94$: (*a*) $R = R_c = 121.67$, $\lambda_R = 446.76$; (*b*) $R = R_{c2} = 124.08$, $\lambda_R = 85.02$; (*c*) $R = R_{c2} = 124.08$, $\lambda_R = 15.98$.

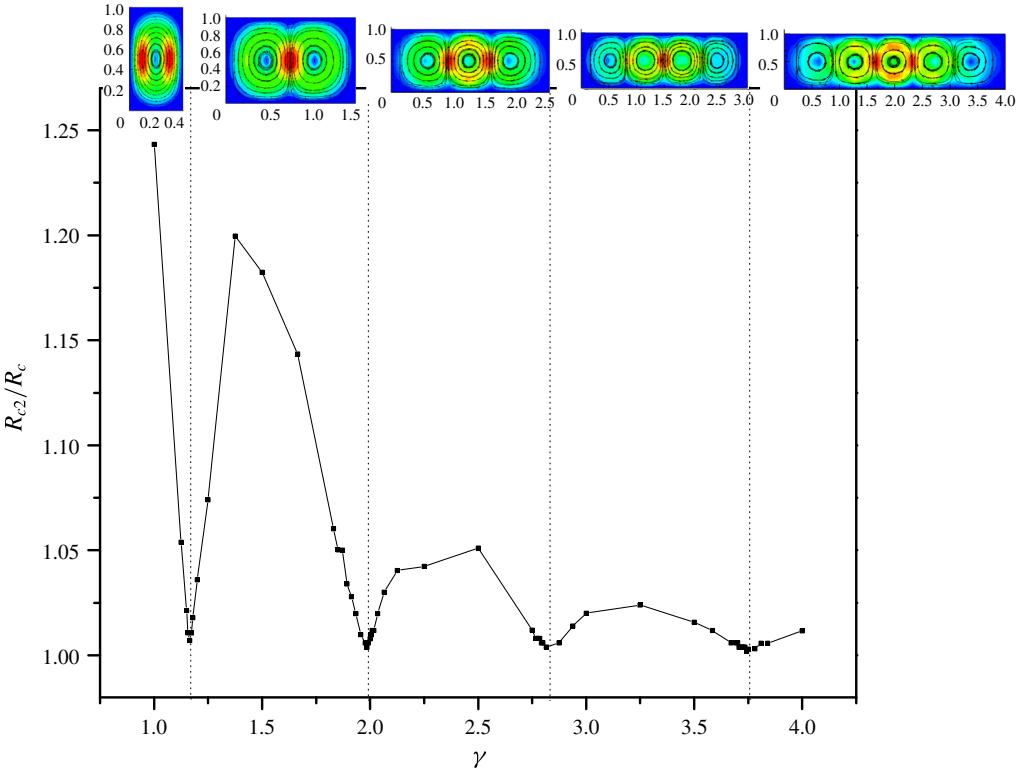

FIGURE 9. (Colour online) The variation of R_{c2}/R_c with respect to the film aspect ratio.

behaviour between six-cell and eight-cell flow patterns in electroconvection within a small-aspect-ratio cell. Pfister *et al.* (1988) also observed transition between different bifurcation branches in Taylor–Couette flow in a very short annulus.

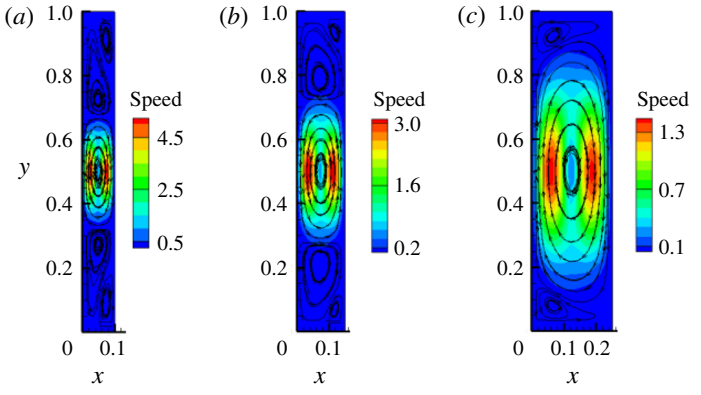

FIGURE 10. (Colour online) Flow patterns obtained from stability analysis for very small aspect ratios: (*a*) $R = R_c = 10385.8$, $\gamma = 0.10$; (*b*) $R = R_c = 4205.8$, $\gamma = 0.15$; (*c*) $R = R_c = 1224.1$, $\gamma = 0.25$.

As the aspect ratio of the film decreases below 1, flow patterns with distributions in the y direction can also be obtained from stability analysis, as shown in figure 10. This flow structure development along the y direction is not as regulated as that in the x direction. A multiple-vortex pattern as observed in the x direction cannot be obtained in the y direction. Moreover, these flow patterns with very low aspect ratios cannot be observed from the current experiment and have not been reported in any previous experimental works. As can be noted in figure 10, the critical R numbers are extremely high compared with those calculated under larger aspect ratios (as shown in figure 6). Therefore, the driving voltages for these liquid films with small aspect ratios are very high, which makes experiment unrealizable.

5. Conclusions

In this work, the electroconvection problem of a suspended liquid crystal film with a rectangular boundary was investigated. Global stability analysis was carried out to extract the resulting flow patterns on the film for different aspect ratios when the applied DC voltage reached critical values. The obtained flow patterns were well validated by PIV experiment. The variation of the critical voltage (R number) with respect to the film aspect ratio was also obtained in the stability analysis. It was found that the critical voltage (R number) decreases almost exponentially fast in the low-aspect-ratio region ($\gamma < 1.5$), and then the variation becomes very slow. Moreover, the variation process of the flow pattern on the film as the aspect ratio gradually increases was described using stability analysis results. In the current experiment, the flow pattern was observed to be unstable at certain aspect ratios, as mentioned in earlier works by Faetti *et al.* (1983) and Mao *et al.* (1996). This phenomenon was explained by the occurrence of parallel unstable eigenmodes in the stability analysis. The flow structure development along the vertical direction (y direction) was also obtained in the stability analysis for small aspect ratios ($\gamma < 1$).

Acknowledgements

This research is supported by Shanghai Yangfan Plan (no. 14YF1400200), Shanghai Chenguang Plan (no. 13CG01) and Fudan's Undergraduate Research Opportunities

Program (no. 15101). The authors acknowledge T. Xu from Beijing MicroVec Ltd. for his guidance and help in the PIV experiment. The authors are also grateful to Professor L. Zhou, Professor C. Tian, Professor Y. Wu and Professor J. Xu for their interesting discussions, and would like to thank A. Li for her help in the experimental set-up.

REFERENCES

BECKER, A., RIED, S., STANNARIUS, R. & STEGEMEYER, H. 1997 Electroconvection in smectic C liquid-crystal films visualized by optical anisotropy. *Europhys. Lett.* **39** (3), 257–262.

BINKS, D. J. & MULLIN, T. 1997 Cell number selection in electrohydrodynamic convection in liquid crystals. *Proc. R. Soc. Lond.* A **453** (1965), 2109–2122.

BUKA, Á., ÉBER, N., PESCH, W. & KRAMER, L. 2007 Isotropic and anisotropic electroconvection. *Phys. Rep.* **448** (5), 115–132.

CROSS, M. C. & HOHENBERG, P. C. 1993 Pattern formation outside of equilibrium. *Rev. Mod. Phys.* **65** (3), 851–1112.

DAYA, Z. A., DEYIRMENJIAN, V. B. & MORRIS, S. W. 1999 Electrically driven convection in a thin annular film undergoing circular Couette flow. *Phys. Fluids* **11** (12), 3613–3628.

DAYA, Z. A., DEYIRMENJIAN, V. B. & MORRIS, S. W. 2002 Sequential bifurcations in sheared annular electroconvection. *Phys. Rev.* E **66** (1), R015201.

DAYA, Z. A., MORRIS, S. W. & BRUYN, J. R. 1997 Electroconvection in a suspended fluid film: a linear stability analysis. *Phys. Rev.* E **55** (3), 2682–2692.

FAETTI, S., FRONZONI, L. & ROLLA, P. A. 1983 Static and dynamic behavior of the vortexelectrohydrodynamic instability in freely suspended layers of nematic liquid crystals. *J. Chem. Phys.* **79** (10), 5054–5062.

FEIZ, M. S., NAMIN, R. M. & AMJADI, A. 2015 Theory of the liquid film motor. *Phys. Rev.* E **92**, 033002.

KRAMER, L. & PESCH, W. 1995 Convection instabilities in nematic liquid crystals. *Annu. Rev. Fluid Mech.* **27**, 515–541.

MAO, S. S., BRUYN, J. R., DAYA, Z. A. & MORRIS, S. W. 1996 Boundary-induced wavelength selection in a one-dimensional pattern-forming system. *Phys. Rev.* E **54** (2), R1048–1051.

MELCHER, J. R. & TAYLOR, G. I. 1969 Electrohydrodynamics: a review of the role of interfacial shear stresses. *Annu. Rev. Fluid Mech.* **1** (5), 111–146.

MORRIS, S. W., BRUYN, J. R. & MAY, A. D. 1990 Electroconvection and pattern formation in a suspended smectic film. *Phys. Rev. Lett.* **65** (19), 2378–2381.

MORRIS, S. W., BRUYN, J. R. & MAY, A. D. 1991 Velocity and current measurements in electroconvecting smectic films. *Phys. Rev.* A **44** (12), 8146–8157.

PATRÍCIO, P., LEAL, C. R., PINTO, L. F. V., BOTO, A. & CIDADE, M. T. 2012 Electro-rheology study of a series of liquid crystal cyanobiphenyls: experimental and theoretical treatment. *Liq. Cryst* **39** (1), 25–37.

PÉREZ, A. T., VÁZQUEZ, P. A., WU, J. & TRAORÉ, P. 2014 Electrohydrodynamic linear stability analysis of dielectric liquids subjected to unipolar injection in a rectangular enclosure with rigid sidewalls. *J. Fluid Mech.* **758**, 586–602.

PFISTER, G., SCHMIDT, H., CLIFFE, K. A. & MULLIN, T. 1988 Bifurcation phenomena in Taylor–Couette flow in a very short annulus. *J. Fluid Mech.* **191**, 1–18.

SHARMA, D., MACDONALD, J. C. & IANNACCHIONE, G. S. 2006 Thermodynamics of activated phase transitions of 8CB: DSC and MC calorimetry. *J. Phys. Chem.* B **110**, 16679–16684.

TRAORÉ, P. & PÉREZ, A. T. 2012 Two-dimensional numerical analysis of electroconvection in a dielectric liquid subjected to strong unipolar injection. *Phys. Fluids* **24**, 037102.

TSAI, P., DAYA, Z. A., DEYIRMENJIAN, V. B. & MORRIS, S. W. 2007 Direct numerical simulation of supercritical annular electroconvection. *Phys. Rev.* E **76** (2), 026305.

TSAI, P., DAYA, Z. A. & MORRIS, S. W. 2004 Aspect-ratio dependence of charge transport in turbulent electroconvection. *Phys. Rev. Lett.* **92** (8), 084503.

TSAI, P., MORRIS, S. W. & DAYA, Z. A. 2008 Localized states in sheared electroconvection. *Europhys. Lett.* **84** (1), 14003.